Solar convection simulations using a B-spline method

By T. Hartlep AND N. N. Mansour

1. Motivation and objectives

Convection plays a key role in energy transport and global circulation in the outer layers of the Sun, in generation of solar magnetic fields and in many phenomena associated with solar activity and variability. Observations of the solar surface reveal structures that have been classified as granules, mesogranules, and supergranules. The nomenclature reflects organization at three spatial scales ranging from about 1 Mm to 30 Mm.

Numerical simulations of the near surface region of the Sun (Stein & Nordlund 2000) capture structures on the granular scale, but have not been able to detect organization at large scales. The physical mechanism of supergranulation is presently unknown. It has been suggested that supergranulation corresponds to a large convective cells which develop due to enhanced convective instability in the HeII ionization layer. This layer lies deeper than Stein & Nordlund have investigated so far.

We know that as we go deeper from the surface of the sun, the turbulence structures become large, and the Mach number decreases. It is then advantageous to be able to change the spatial resolution in all three coordinates as a function of depth. In addition, it is numerically advantageous to use the anelastic approximation (Ogura & Phillips 1962; Gough 1969; Gilman & Glatzmaier 1981) to the compressible Navier-Stokes equations for deep domains. Using B-splines in one coordinate direction and Fourier methods in the other two coordinate directions, Kravchenko *et al.* (1996) and Loulou *et al.* (1997) have developed B-spline–spectral numerical schemes that enable changing the resolution as a function of height. Kravchenko *et al.* (1996) applied the scheme to simulate the fully developed turbulent channel flow by resolving the near-wall region and relaxing the resolution in the core region. Loulou *et al.* (1997) simulated a fully developed turbulent pipe flow. They applied the scheme to remove the centerline singularity in cylindrical coordinates.

2. Numerical method

Under this effort, a new code to simulate a rectilinear section of the solar convection zone is being implemented. As a first step, the numerical method is implemented for a simple Boussinesq fluid (Oberbeck 1879; Boussinesq 1903) and is presented in this paper for this case only. Later, once the new code is fully functional and tested, equations based on the anelastic approximation will be used.

2.1. *Basic equations*

Using the temperature difference across the fluid layer, ΔT, the layer thickness d and the thermal diffusion time d^2/κ as units of temperature, length and time, the dimensionless Boussinesq equations read:

$$\partial_t \vec{v} + (\vec{v} \cdot \nabla)\vec{v} = -\nabla\pi + Pr\nabla^2\vec{v} + RaPr\theta\vec{e}_z, \tag{2.1}$$

$$\partial_t \theta + (\vec{v} \cdot \nabla)\theta = \nabla^2 \theta + \vec{v} \cdot \vec{e}_z, \tag{2.2}$$

$$\nabla \cdot \vec{v} = 0. \tag{2.3}$$

$\vec{v}$, θ and π denote the velocity of the fluid and the deviations of the temperature and pressure from their static profiles, i.e. the temperature and pressure profiles that would be observed in the case of no motion. The equations contain two dimensionless parameters: the Prandtl number Pr and the Rayleigh number Ra, which are defined as

$$Pr = \frac{\nu}{\kappa}, \quad Ra = \frac{g\alpha \Delta T d^3}{\kappa \nu}, \tag{2.4}$$

with κ, ν, α and g being the coefficients of thermal conductivity, kinematic viscosity and thermal expansion, and the accelleration due to gravity, which points in negative z direction. The Boussinesq approximation assumes all these properties to be constant throughout the layer.

2.2. *Velocity decomposition*

A poloidal/toroidal decomposition is used for the velocity to automatically fulfill the continuity equation $\nabla \cdot \vec{v} = 0$. Even though the divergence of the velocity does not vanish in the anelatic approximation, the equations that we are ultimately going to use, such a representation can still be used. Just not for the velocity itself, but for the quantity $\rho_0 \vec{v}$, where ρ_0 denotes the reference density.

In the Boussinesq case, the representation is in the form of

$$\vec{v}(x,y,z,t) = \nabla \times [\psi(x,y,z,t)\vec{e}_z] + \nabla \times \nabla \times [\phi(x,y,z,t)\vec{e}_z] + \vec{U}(z,t). \tag{2.5}$$

In this way the poloidal and toroidal scalars ϕ and ψ are periodic in x and y, and $\vec{U}$ represents the horizontal average of the velocity, i.e

$$\vec{U}(z,t) = \left\langle \vec{v}(x,y,z,t) \right\rangle_{x,y}. \tag{2.6}$$

The z component of $\vec{U}$ must be zero to satisfy the continuity equation. $\vec{U}$ is thus a toroidal flow. However, the corresponding toroidal scalar varies linearly in x and y and is unbounded. Obviously, we require ϕ to be periodic and to remain finite in the numerical representation. Therefore $\vec{U}$ needs to be included in the decomposition of $\vec{v}$ (Schmitt & von Wahl 1992).

Equations of motion for ϕ, ψ and $\vec{U}$ can be derived by evaluating the z component of the curl of the curl of (2.1), the z component of the curl of (2.1) and the horizontal average of (2.1), respectively.

2.3. *Spectral method for the horizontal directions*

Periodic boundary conditions are used in the horizontal directions to reduce the influence of the horizontal boundaries on the flow. A natural choice is the use of Fourier modes in those directions, i.e.

$$f(x,y,z,t) = \sum_{\vec{k}} \hat{f}_{\vec{k}}(z,t) e^{-i(k_x x + k_y y)} \qquad (f = \phi, \psi, \theta), \tag{2.7}$$

with $\vec{k} = k_x \vec{e}_x + k_y \vec{e}_y$ being the horizontal wave vector. Multiplying the equations of motion with weight functions $e^{i(k'_x x + k'_y y)}$ and integrating over the entire horizontal plane then yields equations for the z and t dependent Fourier coefficients:

$$[\partial_z^2 - k^2]\Big[\partial_t - Pr[\partial_z^2 - k^2]\Big]\hat{\phi}_{\vec{k}}(z,t) = \mathcal{R}_{\hat{\phi}_{\vec{k}}}(z,t), \tag{2.8}$$

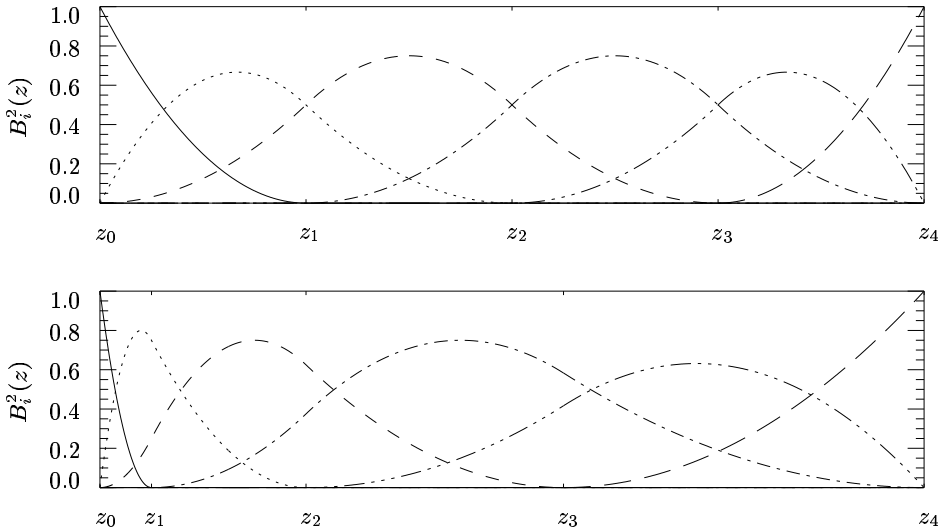

FIGURE 1. Second-order B-splines defined on sets of 5 knot point in the case of equally spaced knot points (top diagram) and non-equally spaced knot points (bottom diagram). In both cases solid, dotted, dashed, dash-dotted, dash-dot-dotted and long-dashed lines denote splines $B_1^2, \ldots, B_6^2$, respectively.

$$\left[\partial_t - Pr[\partial_z^2 - k^2]\right]\hat{\psi}_{\vec{k}}(z,t) = \mathcal{R}_{\hat{\psi}_{\vec{k}}}(z,t), \tag{2.9}$$

$$\left[\partial_t - [\partial_z^2 - k^2]\right]\hat{\theta}_{\vec{k}}(z,t) = \mathcal{R}_{\hat{\theta}_{\vec{k}}}(z,t). \tag{2.10}$$

All non-linear terms are contained in the right-hand sides $\mathcal{R}$. The equation for $\vec{U}$ is very similar:

$$[\partial_t - Pr\partial_z^2]\vec{U}(z,t) = \mathcal{R}_{\vec{U}}(z,t). \tag{2.11}$$

If fact, we can discuss the equation for $\hat{\psi}_{\vec{k}}$, $\hat{\theta}_{\vec{k}}$ and $\vec{U}$ together, since they all can be written in the form

$$[\partial_t + C_0 - C_2\partial_z^2]f(z,t) = \mathcal{R}_f(z,t) \qquad (f = \hat{\psi}_{\vec{k}}, \hat{\theta}_{\vec{k}}, \vec{U}), \tag{2.12}$$

with some parameters C_0 and C_2.

2.4. *B-spline method for the vertical direction*

Spatial discretization in the vertical direction z is done by a B-spline method (Kravchenko & Moin 1998), i.e. the unknowns, $\hat{\phi}_{\vec{k}}, \hat{\psi}_{\vec{k}}, \hat{\theta}_{\vec{k}}$ and $\vec{U}$, are expanded in terms of m-order piecewise polynomials called basis splines, or B-splines. With a given set of knot points $\{z_0, \ldots, z_N\}$ that divide the z domain into N subintervals, one can construct $N + m$ of these spline functions using the recursive expression

$$B_j^m(z) = \frac{z - z_{j-m-1}}{z_{j-1} - z_{j-m-1}} B_{j-1}^{m-1}(z) + \frac{z_j - z}{z_j - z_{j-m}} B_j^{m-1}(z) \qquad (j = 1, \ldots, N + m). \tag{2.13}$$

Here, B_j^m denotes the j-th B-spline of order m. The 0-order splines are given by

$$B_j^0(z) = \begin{cases} 1 & \text{if } z_{j-1} \leq z \leq z_j \\ 0 & \text{otherwise} \end{cases} . \tag{2.14}$$

As it turns out, m additional points at each side of the domain ($z_{-m}, \ldots, z_{-1}$ and $z_{N+1}, \ldots, z_{N+m}$) are needed in the construction of B-splines near the boundaries. These virtual points are chosen to be equal to the boundary points z_0 and z_N, i.e. $z_{-m} = \ldots = z_{-1} = z_0$ and $z_{N+m} = \ldots = z_{N+1} = z_N$.

Second-order B-spline functions for two different sets of knot points are shown in figure 1 to illustrate how these functions look like. As can be seen from the figure, B-splines have compact support and are non-negative:

$$B_j^m(z) \begin{cases} > 0 & \text{if } z_{j-m-1} < z < z_j \\ = 0 & \text{otherwise} \end{cases} , \tag{2.15}$$

and can be tuned to the specific needs at hand by the choice of knot points. In areas where small structures need to be resolve, e.g. in boundary layers, one can choose closely spaced knot points, while in areas where such high resolution is not required, the grid can be coarse to save computational costs.

Incorporating a B-spline expansion of the unknowns, i.e.

$$f(z,t) = \sum_{j=1}^{N+m} \alpha_{f,j}(t) B_j^m(z) \qquad (f = \hat{\phi}_{\vec{k}}, \hat{\psi}_{\vec{k}}, \hat{\theta}_{\vec{k}}, \vec{U}), \tag{2.16}$$

into the governing equations (2.8) and (2.12), multiplying with weight functions B_i^m and integrating over the z domain yields equations for the expansion coefficients $\alpha_{f,j}(t)$:

$$\sum_{j=1}^{N+m} \left[(\partial_t + C_0) \left(\mathcal{M}_0 \right)_i^j - C_2 \left(\mathcal{M}_2 \right)_i^j \right] \alpha_{f,j} = \int B_i^m \mathcal{R}_f dz \qquad (f = \hat{\psi}_{\vec{k}}, \hat{\theta}_{\vec{k}}, \vec{U}), \tag{2.17}$$

$$\sum_{j=1}^{N+m} \left[-(k^2 \partial_t + k^4 Pr) \left(\mathcal{M}_0 \right)_i^j + (\partial_t + 2k^2 Pr) \left(\mathcal{M}_2 \right)_i^j - Pr \left(\mathcal{M}_4 \right)_i^j \right] \alpha_{\hat{\phi}_{\vec{k}},j} = \int B_i^m \mathcal{R}_{\hat{\phi}_{\vec{k}}} dz. \tag{2.18}$$

Three matrices, $\mathcal{M}_0$, $\mathcal{M}_2$ and $\mathcal{M}_4$, occur in these equations, which contain integrals of the product of two B-splines and the product of a B-spline with a derivative of a B-spline:

$$\left(\mathcal{M}_n \right)_{i=1,\ldots,N+m}^{j=1,\ldots,N+m} = \int B_i^m \partial_z^n B_j^m dz \qquad (n = 0, 2, 4). \tag{2.19}$$

It follows from the property (2.15) that all of these matrices are of band-diagonal form. Specifically, they have only m subdiagonals and m superdiagonals which contain non-zero entries.

2.5. *Time advancement*

A mixed implicit/explicit method using a Crank-Nicolson scheme for the diffusive terms and a second-order Adams-Bashforth scheme for the advection and buoyancy terms is used for the time advancement.

In the end, one has to solve a matrix equation for each Fourier mode of each field (poloidal, toroidal, mean flow and temperature) in the form

$$\mathcal{N}_f \vec{a}_f = \vec{b}_f, \tag{2.20}$$

with $\vec{a}_f$ representing the vector of B-spline coefficients at the new time step t_{n+1}, i.e. $\vec{a}_f = (\alpha_{f,1}(t_{n+1}), \ldots, \alpha_{j,N+m}(t_{n+1}))$ (f again stands for either $\hat{\phi}_{\vec{k}}$, $\hat{\psi}_{\vec{k}}$,$\hat{\theta}_{\vec{k}}$ or $\vec{U}$), and the matrix $\mathcal{N}_f$ is composed of the previously introduced matrices $\mathcal{M}_0$, $\mathcal{M}_2$ and $\mathcal{M}_4$. $\mathcal{N}_f$ is therefore band-diagonal and a fast method for solving band-diagonal systems can be used.

2.6. *Imposing boundary conditions*

So far, no boundary conditions have been imposed in the vertical direction. Since only one B-spline, and the derivative of only two B-splines are non-zero at the boundary, it is rather easy to implement various boundary conditions. If for example one needs to prescribe the value of $f(z,t)$ at the boundary z_0, e.g. $f(z = z_0, t) = g(t)$, one simply has to set the first B-spline coefficient to that value, i.e. $\alpha_{f,1}(t) = g(t)$. The original equation for $\alpha_{f,1}$ has to be removed from the linear system (2.20), and $\alpha_{f,1}$'s contribution has to be deducted from the right hand, i.e. equation (2.20) is modified in the following way:

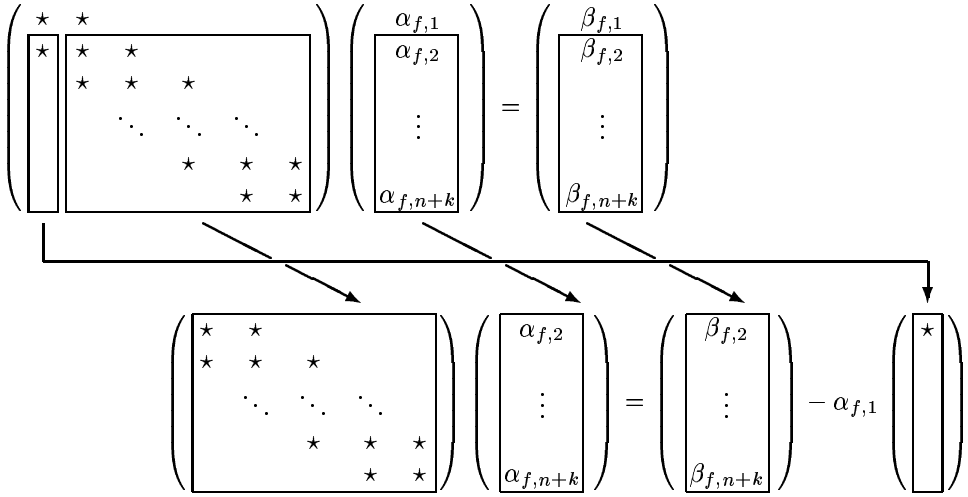

More complicated boundary conditions in which the value of the B-spline coefficients at the boundary depend on the coefficients in the interior can be implemented by directly manipulating the matrix elements of $\mathcal{N}_f$.

2.7. *Varying numerical resolution with depth*

The main advantage of such a B-spline method is the ability to vary the spatial resolution in all directions as a function of depth. As already mentioned, the choice of knot points in the construction of the B-spline functions determines the vertical resolution. Near the surface of the sun, where high spatial resolution is required, closely spaced knot points will be chosen, while the spacing can be increased in deeper parts of the convection zone. The spatial resolution in horizontal directions is determined by the number of Fourier modes that one wants to consider in the discretization:

$$f(x,y,z,t) = \sum_j \sum_{\vec{k}} \alpha_{f,j}(t) e^{-i(k_x x + k_y y)} B_j^m(z) \qquad (f = \phi_{\vec{k}}, \psi_{\vec{k}}, \theta_{\vec{k}}), \tag{2.21}$$

and this number can be changed from one spline index j to the next. Since according to (2.15) B-splines of different j overlap, the change in resolution occurs over several knot points. A consequence of the variation of horizontal resolution is, that for a given set of

wavenumbers k_x and k_y only a subset of B-splines has to be considered, namely those for which the maximum wavenumbers that we have chosen are larger or equal to k_x and k_y. The other coefficients are zero and the corresponding rows and columns in the matrix equations (2.20) can therefor be dropped to reduce the numerical cost.

3. Future work

The implementation of the presented numerical method is nearly complete and will be tested shortly for some test cases of turbulent Rayleigh-Bénrad convection. Comparisons will be done with the results obtained by Hartlep (2004) using a Chebyshev method. After that, the anelastic equations will be implemented in place of the Boussinesq equations.

The final ingredient for the solar simulations is the definition of reasonable boundary conditions. As a start, we can use rather simple conditions like the ones used by Miesch (1998) and others: stress-free, impenetrable upper und lower boundaries with constant heat flux at the bottom and constant entropy at the top of the computational domain. A refinement to these boundary conditions would be the treatment of the upper surface as a free surface, which could be realized by additionally tracking a height function $h(x, y, t)$ above the top end of the discretization (2.21).

REFERENCES

BOUSSINESQ, J. 1903 *Theorie Analytique de la Chaleur*, vol. 2. Paris: Gauthier-Villars.

GILMAN, P. & GLATZMAIER, G. A. 1981 Compressible convection in a rotating spherical shell. I. Anelastic equations. *Astrophys. J. Suppl.* **45**, 335–388.

GOUGH, D. O. 1969 The anelastic approximation for thermal convection. *J. Atmos. Sci.* **26**, 448–456.

HARTLEP, T. 2004 *Strukturbildung und Turbulenz. Eine numerische Studie zur turbulenten Rayleigh-Bénard Konvektion*. Doctoral thesis. Institute of Geophysics, University of Göttingen.

KRAVCHENKO, A. G. & MOIN, P. 1998 *B-spline methods and zonal grids for numerical simulations of turbulent flows*. Report No. TF-73, Department of Mechanical Engineering, Stanford University.

KRAVCHENKO, A. G., MOIN, P. & MOSER, R. 1996 Zonal embedded grids for numerical simulations of wall-bounded turbulent flows. *J. Comp. Phys.* **127(2)**, 412–423.

LOULOU, P., MOSER, R. D., MANSOUR, N. N. & CANTWELL, B. J. 1997 *Direct numerical simulation of incompressible pipe flow using a B-Spline Spectral Method*. Technical Memorandum 110436, NASA Ames Research Center.

MIESCH, M. S. 1998 *Turbulence and convection in stellar and interstellar enviroments*. PhD thesis. Department of Astrophysical and Planetary Sciences, University of Colorado.

OBERBECK, A. 1879 Über die Wärmeleitung der Flüssigkeiten bei Berücksichtigung der Strömungen infolge von Temperaturdifferenzen. *Ann. Phys. Chem.* **7**, 271–292.

OGURA, Y. & PHILLIPS, N. A. 1962 Scale analysis of deep and shallow convection in the atmosphere. *J. Atmos. Sci.* **19**, 173–179.

SCHMITT, B. J. & VON WAHL, W. 1992 Decomposition into poloidal fields, toroidal fields, and mean flow. *Differential and Integral Equations* **5**, 1275–1306.

STEIN, R. F. & NORDLUND, A. 2000 Realistic solar convection simulations. *Solar Phys.* **192**, 91–108.